FUDMA Journal of Sciences (FJS)
ISSN online: 2616-1370
ISSN print: 2645 - 2944
Vol. 6 No. 6, December, 2022, pp 336 - 353
DOI: https://doi.org/10.33003/fjs-2022-0606-1310

VALIDATION OF EXTENDED ELASTIC IMPEDANCE BASED ON MINIMUM ENERGY ANGLE. A CASE STUDY APPLICATION FOR OPTIMIZED PETROLEUM RESERVOIR CHARACTERIZATION

[*1]Muhktar Habib, [1]Bashir Aliyu Abba, [1]Aminu Uba Alhassan and [2]Jibia Firdausi Umar

[1]Department of Petroleum and Gas Processing Engineering, Kaduna Polytechnic, Nigeria.
[2]Department of Physical Planning, Umaru Musa Yaradua University, Katsina, Nigeria.

*Corresponding authors' email: mukhtarhabib102@gmail.com

ABSTRACT

This work intends to showcase a validation of the applicability of Extended Elastic Impedance (EEI) inversion method in reservoir characterization and modeling. In order to achieve that, deterministic seismic inversion and extended elastic impedance (EEI) analysis were applied to obtain quantitative estimates of reservoir properties over the Pu field of the West African Congo basin. Optimum EEI angles corresponding to the reservoir properties were then analyzed using well logs data, together with a lithology indicator. Pre-stack seismic data were simultaneously inverted into density, acoustic and gradient impedances cubes, through model based inversion algorithm. The last two broadband inverted volumes were then projected to corresponding Chi angles proportionate to petrophysical indicators, thus resulting to two broadband EEI volumes. At well locations, the EEI versus petrophysical parameters linear trends were then applied to convert EEI volumes into porosity and shale volumes based on specified lithology. In order to generate reservoir facies distribution, minimum angle was applied based on background EEI, thus allowing for mapping of reservoir facies. In order to validate the EEI approach, a Geo-statistical model was further developed for the same field. Hence, from porosity, shale content and background EEI cubes, a comparison was made between the properties generated from the EEI and that generated based on geo-statistical method, which shows that EEI is a robust way of reservoir characterization that pinpointing favorable reservoir potentials which shall guide future drilling locations.

Keywords: Extended Elastic Impedance, Reservoir Geo-statistical model, Minimum Energy Angle and Facies

INTRODUCTION

A reliable quantitative measurement of petrophysical parameters, such as porosity, shale volume, water saturation coupled with distribution of reservoir characteristics in 3D space are considered as key objectives in the Pu field of West African Congo Basin. A proper understanding of sand body distribution is vital for well planning and production enhancement. As a result, measurement of relevant petrophysical parameters such as shale volume (V_{sh}), effective water saturation (S_w) and porosity are of great importance for static modeling and reserve estimation. These three reservoir properties are usually derived from Seismic impedances (P and S- impedance) data through either classical statistical modeling of rock properties and elastic properties derived from well logs (Dubucq, 2001; Vernik, 2002), or geo-statistical approach (Doyen, 2009).

In this work, the concept of EEI (extended elastic impedance) was applied on a West African field. The is based on selection guided by the thickness of targeted reservoirs, largely above the tuning thickness. The concept was applied to derive three major petrophysical properties that are basically targeted at different reservoir units and also in order to map the distribution of reservoir facies in 3D space. After a careful comparison with results derived from conventional geostatistics, it was discovered that EEI corresponding to minimum energy χ is a reliable method for extraction of spatial distribution of geo-bodies.

This paper presented a scrutiny of the EEI methodology through different Chi angles where the relevant reservoir properties including Porosity (ϕ), Water saturation $(S_{w_{eff}})$ and Shale Volume (V_{sh}) correlate well with EEI logs at $\chi = 22^{o}, 30°$ and $69°$ which was further validated by application of geo-statistical modeling. The primary objective here is to compare properties derived from geo-statistical reservoir model with that of the EEI at minimum energy angle in order to further understand the EEI based reservoir characterization.

Literature Review

Extended Elastic Impedance

The idea of extended elastic impedance is primarily derived from conventional acoustic impedance (AI) inversion which have the central idea of an assumption of a P-Wave impedance from subsurface at normal incidence angle. (Latimar R. B, 2000). This theory perms better in small offset ranges for a CDP gather in which inversion tends to provide reliable result. However, with recent development of amplitude versus offset (AVO), which stronger capability to discriminate hydrocarbon reservoir from the surrounding shale and cap rock, then becomes a rise in demand on analyzing non-zero offset seismic data. (Connolly, 1999), introduced the concept of elastic parameters from non zero offset data from elastic impedance technique. This concept made a breakthrough in the area of fluid discrimination and lithology prediction for many forms of reservoirs, due to its capture of more information on lithology and fluid much more than the conventional acoustic impedance.

Elastic impedance (EI) is therefore a general expression of acoustic impedance based on different incidence angles. It continuously presented a consistent framework to absolutely calibrate and invert non zero offset seismic data. Hence, EI approximation is derived by a linearization of zoeppritz equation, the aki and Richards two term approximation where (θ) is the angle of incidence at reflector interface. Definition of EI is clearly illustrated by (Equations 1. to 4)

$$EI(\theta) = V_p{}^a \times V_s{}^b \times \rho^c \quad (1)$$

Where

$$a = 1 + \sin^2\theta \quad (2)$$

$$b = -8k\sin^2\theta \quad (3)$$

$$c = 1 - 4k\sin^2\theta \quad (4)$$

where

$$K = \left[\frac{V_s}{V_p}\right]^2$$

As shown in Equation 1. the elastic impedance is a function of P-wave velocity (V_p), S-wave velocity (V_s), density (ρ) and incident angle (θ).Factor K is always assumed as constant and usually set to be equal to the average of V_p and V_s over the zone of interest (ZOI)(Connolly, 1999). Connolly 1999 revealed that Elastic Impedance decreases with increase in incident angle when compared to EI at normal incidence (θ). While Connolly's solution provides needed result to some extent that serves as useful guide for optimized petroleum reservoir characterization, a strong restriction of incident angle presented in Equation 1 was a serious challenge and coupled with a key problem of strange unit/dimensions and that values do not scale correctly for different angles (Whitcombe, 2002).

The EI limitations were overcomed by (Whitecombe, 2002) in which he was able to modify Equation 1 by introducing a reference or normalizing constant $\alpha_o, \beta_o, \rho_o$ which represent average value of velocities and density over the zone of interest or value at the top of the target zone. Hence, Whitecombe redefine EI by removing dependence of its dimensionality on the angle (θ). This is out of his realization that some properties of rocks are hard to predict from the existing seismic gathering due to limitations on incidence angle range $(0-30^o)$ in the elastic impedance (Whitecombe, 2002). Meaning that, $\sin^2\theta$ will have to be more than unity in order to estimate some petrophysical properties; however, it is impossible that reflectivity values exceed unity without negative impedance contrast, making it unrealizable (Francis, 2006).

Whitecombe et al (2002) understood that outside the range of $0-30^o$ angle, although EI is not valid for predicting pre-stack seismic data, it is likely to correlate with rock physics or petrophysical properties of interest. Whitecombe et al. (2002) therefore made an extension of EI so that it can be defined for all values of $Sin^2\theta$ between positive and negative infinity. This was achieved after a replacement of $Sin^2\theta$ with $\tan x$ and a subsequent introduction of the notion of scaled reflectivity (normal reflectivity multiplied by $Cosx$). This further results in bounds of the angle x with -90 to $+90^0$. Whitecombe et al. 2002, then made an extensionof the idea of elastic impedance (Connolly, 1999) so that it can be well applied for the purpose of fluid and lithology discrimination. With θ becoming a function called x (Chi angle) which varies between -90^o and 90^o (Figure 1 and Figure 2). Hence, the EEI Equation is expressed as;

$$EEI(x) = \alpha_o\rho_o\left[\left(\frac{\alpha}{\alpha_o}\right)^p\left(\frac{\beta}{\beta_o}\right)^q\left(\frac{\rho}{\rho_o}\right)^r\right] \quad (5)$$

One of the objectives for the development of EEI technique is in order to obtain valuable reflectivity at χ=0° and χ=90° in order to convert it into acoustic and gradient impedances. Thus (Equation 5) can as well be written as;

$$EEI(x) = AI_o\left[\left(\frac{AI}{AI_o}\right)^{\cos x}\left(\frac{GI}{AI_o}\right)^{\sin x}\right] \quad (6)$$

Also, coordinate rotation can also be expressed in log scale as,

$$\log EEI(x) = \log AI_o + \cos x\log\left(\frac{AI}{AI_o}\right) + \sin x\log\left(\frac{GI}{AI_o}\right) \quad (7)$$

Where AI=P-impedance, GI=gradient impedance, α = P-wave velocity, β = S-wave velocity, ρ = Density, $p = \cos x + \sin x$, q = -8Ksinχ and $r = \cos\chi - 4$Ksinχ. AI_0, α_o, β_o *and* ρ_o are average of respective properties used as normalization factors for P-impedance , P velocity, S Velocity and density , respectively. K is the average of $\left(\frac{V_s}{V_p}\right)^2$ in the time depth interval. χ is considered as the rotational angle in the intercept gradient (AB) plane derived from AVO which is related to the angle of incidence θ.

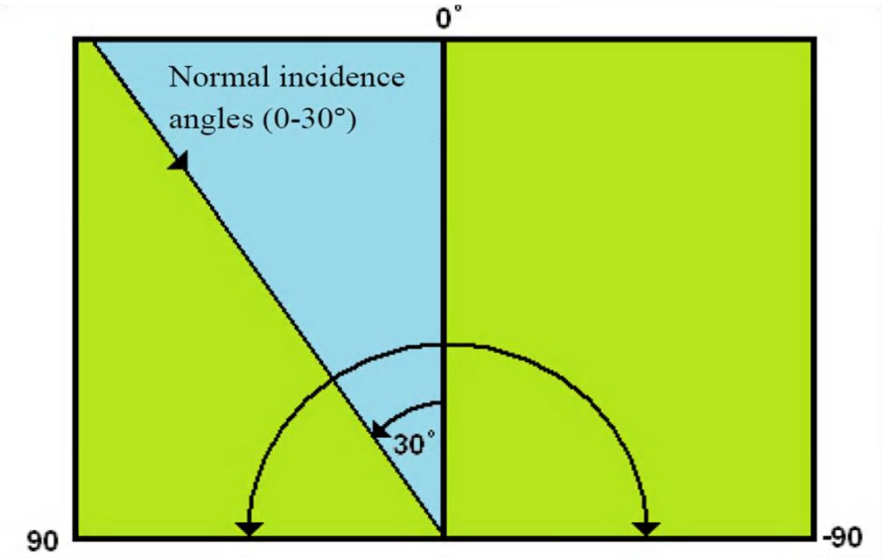

Figure 1: Extended elastic impedance angles can range from -90 to 90, at which values of $\sin^2\theta$ are physically impossible (Hampson-Russell knowledge base,2005)

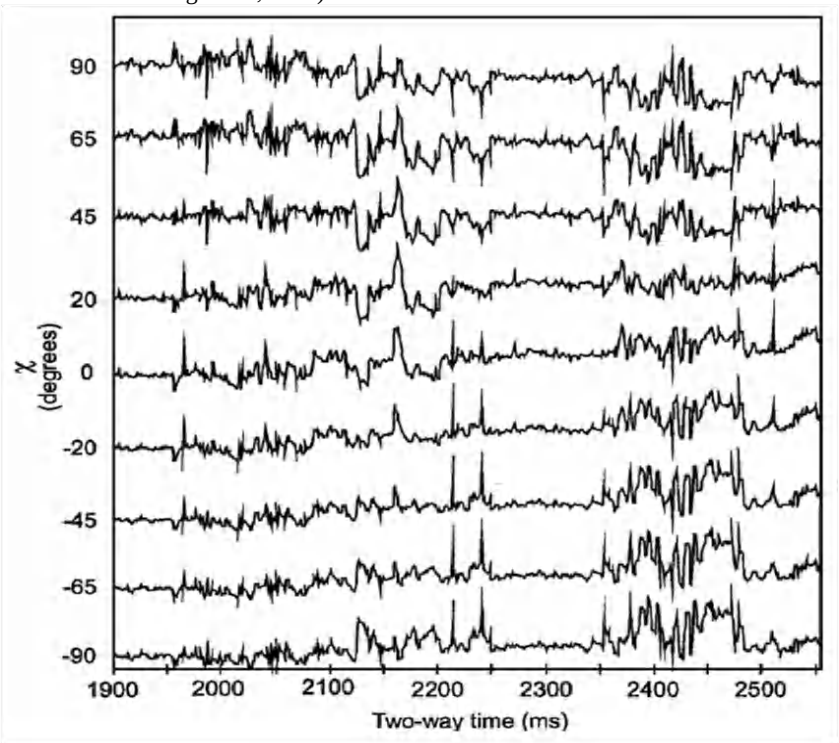

Figure 2: EEI function for various (x) values for a particular well. Note the inverse correlation between EEI ($x = 90^0$) and EEI ($x = -90^o$). (Whitecombe, 2002)

It is now comfortable to state that EEI log at x=0 is similar to EEI log at $\theta = 0$, which simply means acoustic impedance EI. (Whitecombe et al 2002) then developed a robust application for deriving lithology and fluid sensitive seismic impedance volumes. From perspectives of Whitecombe et al 2002, EEI logs at various chi angles are proportional to different rock elastic parameters under certain conditions as depicted by (Figure 3). It can also be stated that a chi angle can be selected to optimize correlation of the EEI logs with reservoir petrophysical values, such as V_{shale}, S_w and porosity, or with elastic parameters. Thus, EEI logs based on specific angles from such parameters can be deducted using EEI equation that is suited for tying well data directly to seismic data (Figure 3). Hence, (Equation 8) is a two term linearization zoeppritz equation mainly for reflectivity (Aki and Richards, 1980).

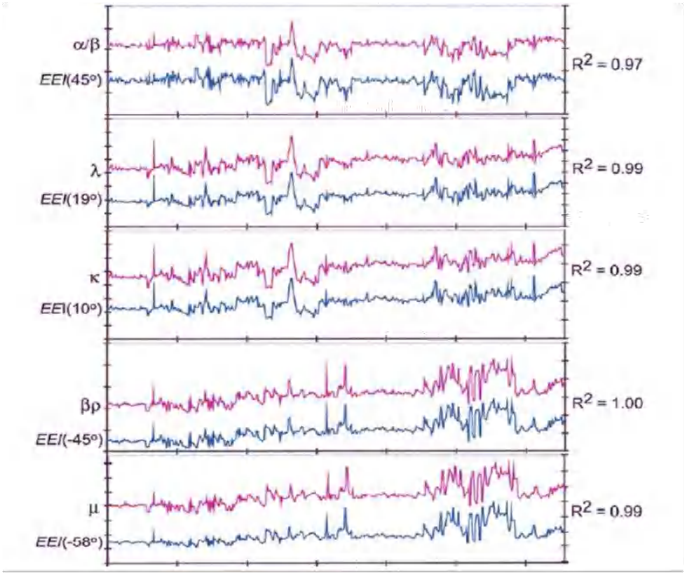

Figure 3: Comparison between elastic parameters and equivalent EEI curve for particular well, representing the high degree of correlation. The EEI function is define as a function of the angle x , not the reflection angle θ . (Whitecombe, 2002)

$$R_p(\theta) = A + B\sin^2\theta \qquad (8)$$

As presented by Whitecombe et al 2002, $\sin^2\theta$ is to be replaced by $\tan x$, so that (Equation 8) becomes (Equation 9), thereby allowing the angle to vary from -90^0 to 90^0

$$R_p(\theta) = A + B\sin^2\theta \Rightarrow R(x) = A + B\tan x \qquad (9)$$

If we assume $x = x_o$ so that $R(\theta)$ is zero in (Equation 9), then it becomes

$$\tan x = -\frac{A}{B} \qquad (10)$$

The angle described by equation 10 is referred to as "Minimum Energy angle" (Hicks, 2006). It is an angle at which reflectivity as defined by two term AVO equation is zero. Figure 4 presents a general concept of EEI inversion approach. As depicted by the flow chart that EEI inversion method consist of building (x) model and inverting an EEI (x) volume based on an inversion algorithm to create an EEI output.

In this work, authors focused mainly on the extended elastic impedance (EEI) based on the simultaneous model based inversion method, conducted to generate several seismic attributes (c $V_p/V_s, LMR$, Poisson ratio, Bulk modulus, Water saturation etc.). A Comparisons of these properties with that of geo-statistics derived rock properties supports the determination of the extent of sensitivity provided by elastic parameters to seismic anomaly, improve reservoir characterization and enhance fluid and lithology imaging.

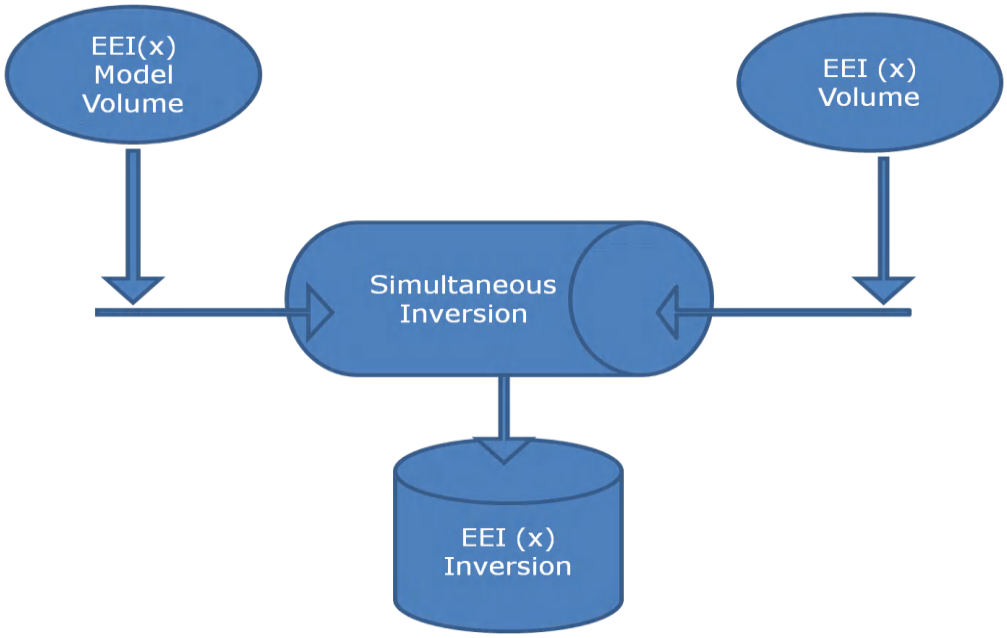

Figure 4a: General concept on extended elastic impedance (EEI) inversion approach (Hampson and Russell knowledge base, 2005)

MATERIALS AND METHODS

This study started with well log data quality control and conditioning, so as toensure that the required data are available and physically reasonable in support of further rock physics activities. A calculation of EEI logs based on various χ angles was done by applying (Equation 5), this was followed by determination of optimum angle that gives the best correlation. A simultaneous model based inversion of prestack time migrated angle partial stacks into acoustic gradient impedanceswas carried out, this include the near (5°-18°), Mid (18°-31°) and far(31° 45°).

Based on the generated optimal angles, computation of equivalent EEI volume through (Equation 9) was done and followed by transformation of EEI volume into quantitative petrophysical property.

Reservoir facies distribution was captured through the concept of minimum energy angle as prescribed by Equation 10. Validation of the EEI approach based on comparison with conventional Geo-statistical method was carried. This was done by first, developing a 3D model of the reservoir based on conventional geostatistical approach and followed by a comparison between the petrophysical properties distribution derived from Geostatistical approach with that derived from the EEI approach.

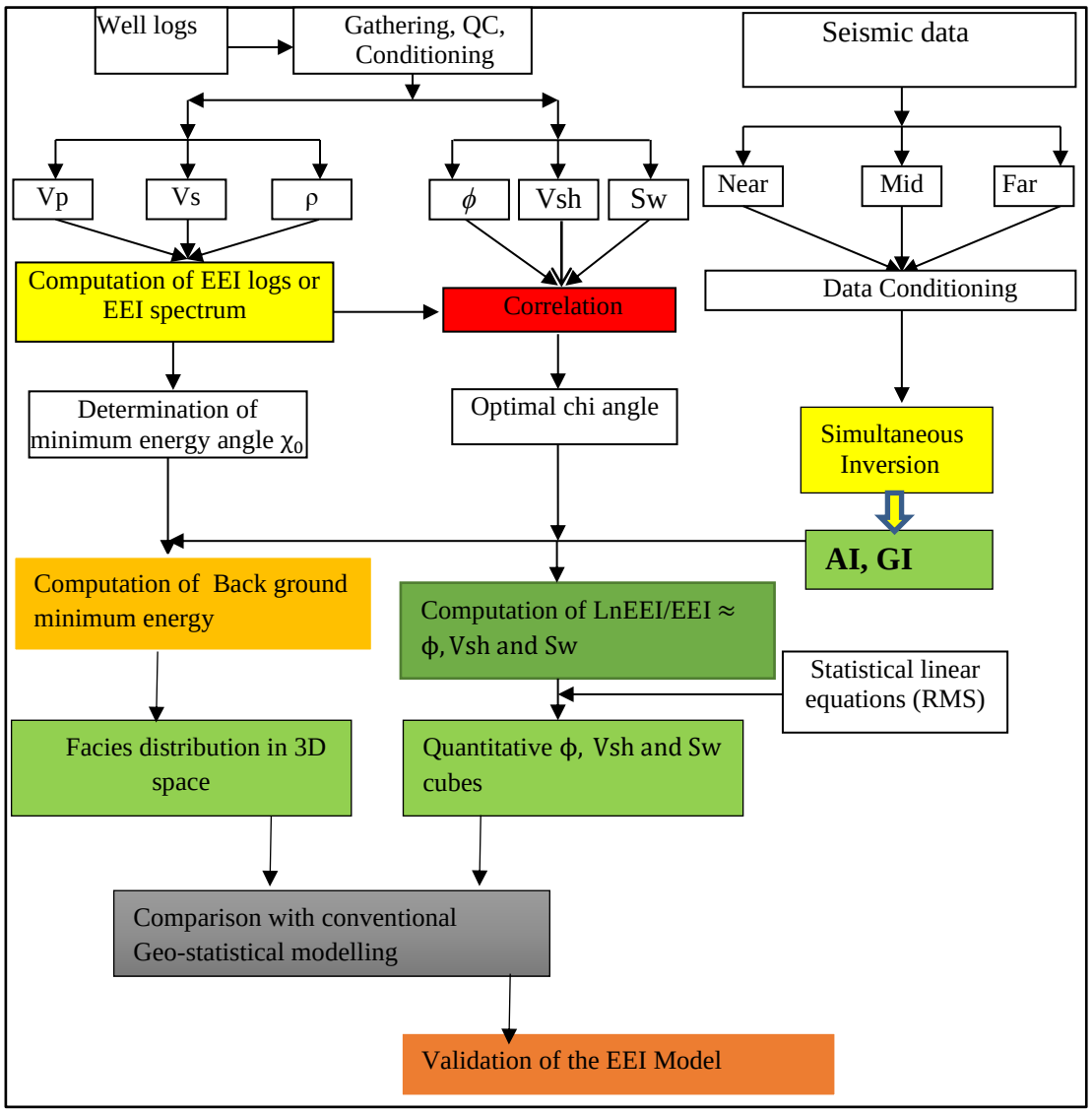

Figure 4b: Pictorial workflow of the methodology

RESULT AND DISCUSSION

Determination of optimum EEI angles

Gathering of well log data and quality assessment:

The well log data and gathering stage ensures that availability of all needed in order to conduct petrophysics and rock physics activities, the operation deals with quality assessment of and improvement of well data, which consist of gaps correction, other identified problems also accounts for possible upscaling. In this research, determined P and S velocities as well as density logs are identified to be of good quality and as depicted in (Figure 5). On (Figure 5a), the red lines representing constant $\frac{V_p}{V_s}$ ratio revealed that values of P and S velocities are in physically reasonable range while the evaluation of multi-well trend plots (Figure 5b) indicated absence of spurious data for the sonic and density.

Computation and correlation of EEI angles

Quality wire line log were applied for the calculation of EEI logs based on (Equation 7) for ranges of $X = -90$ to

$X = +90$. Thus identified correlation between the target log and the EEI logs for every X angle is recorded. Maximum/minimum angles are identified and considered optimal conditions, thereby indicating how well a given petrophysical property can be predicted. The computed EEI logs will be applied during the generation and analysis of EEI log spectrum in order to capture reservoir facies distribution.

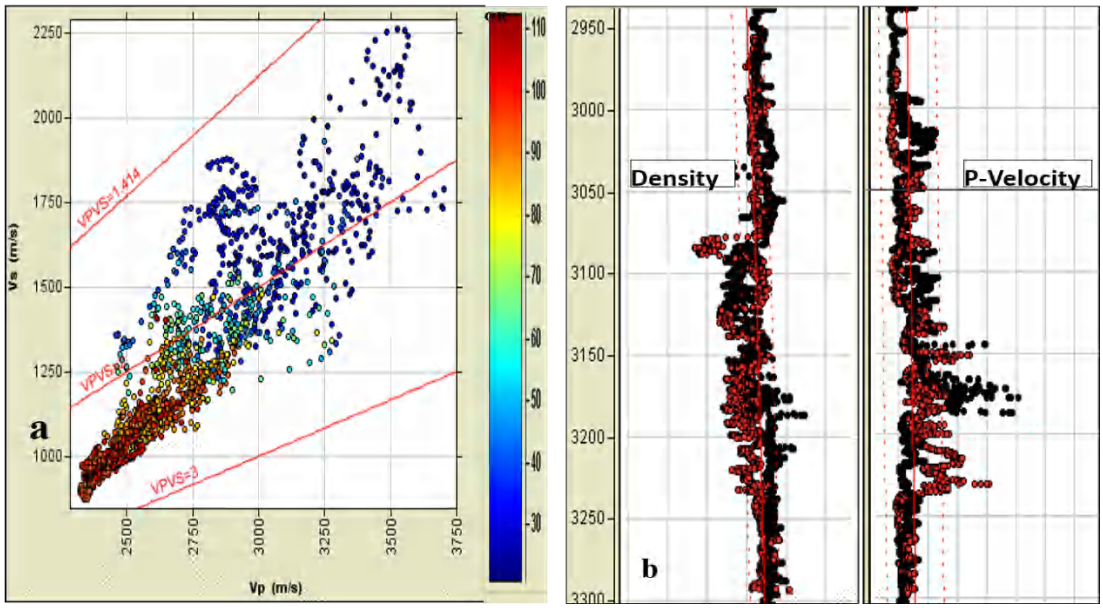

Figure 5: (a) Cross plot of measured P and S velocity with the overlain red lines of constant VpVs ratio, and (b) the evaluation of multi-well trend plots

In this study, an EEI analysis was carried out, where three reservoir properties; Porosity (ϕ), Water saturation $(S_{w_{eff}})$ and Shale Volume (V_{sh}) correlate well with EEI logs at $\chi = 22^{o}, 30°$ and $69°$, respectively. This is depicted in (Figure 6). Despite that other wells are not closely spaced, it can be observed that at each well, EEI corresponding to $\chi = 69^{o}$ or close to it proved a maximum correlation with the shale volume $(V_{sh}\log)$ at a correlation of 86% while EEI corresponding to $\chi = 22^{o}$ or close to it gave a maximum correlation with the porosity log (ϕ) at a correlation of 85%, and EEI corresponding to $\chi = 30^{o}$ or close to it gave a maximum correlation with the effective Water saturation log $(S_{w_{eff}})$ at a correlation of 78%.

Pseudo-petrophysical property logs derived from EEI were developed based on angles of maximum correlation, which gave room for comparison with the corresponding petrophysical well logs as shown in (Figure 7). Thus a good match can be observed between petrophysical parameters and the developed extended elastic impedances (To ease the comparison, both petrophysical and EEI logs were normalized). The matched curves therefore validate any interpretation that is based on the petrophysical volume derived from the EEI based seismic data. The established optimal chi angles will be combined with inverted impedance to generate the respective reservoir petrphysical property cubes in the following sections.

Seismic inversion

Seismic data conditioning and quality assessment

For the well log data, preparation consists of editing and conditioning log curves were needed, an inordinate amount of time can be spent when it comes to seismic data (offset gather). In recent times, seismic partial stacks have become the "evergreen" Pre-stack data as inputs for detailed AVO studies.

In this research, several types of seismic data are available and synthetic seismogram for near and far sections is shown in (Figure 8a) and (Figure 8b). Data was subjected normal quality assessment and control procedure, which did not reveal any severe problems as shown in (Table 1).

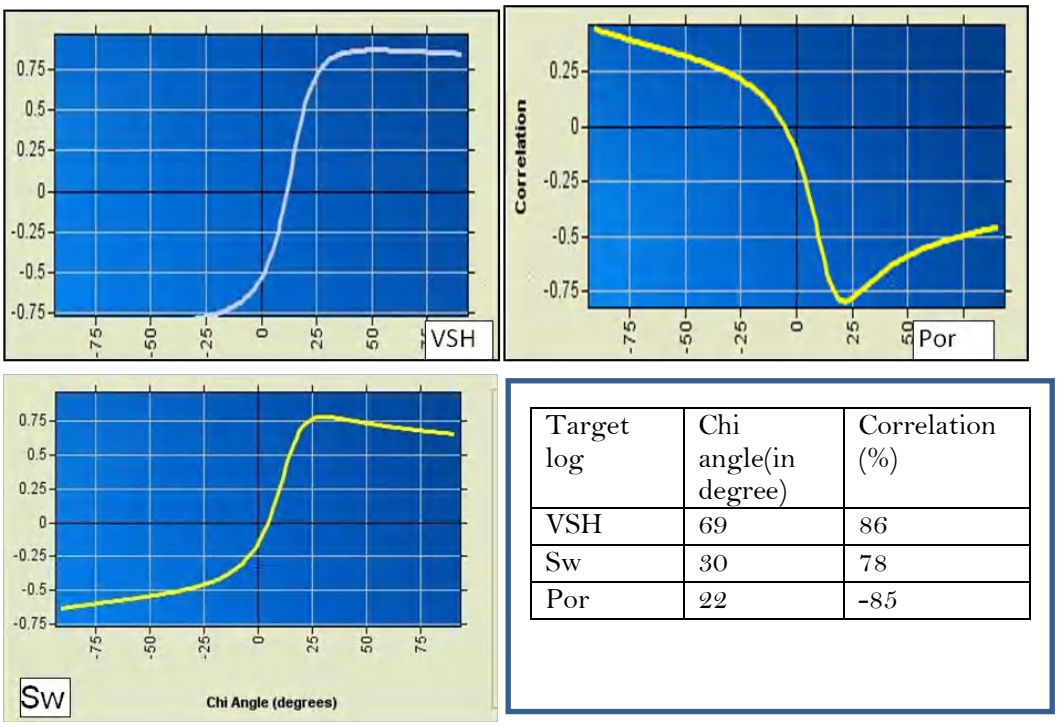

Target log	Chi angle(in degree)	Correlation (%)
VSH	69	86
Sw	30	78
Por	22	-85

Figure 6: Chi angle Correlation for Volume of Shale (V_{sh}), Water Saturation (S_{wt}) and Porosity

Table 1: Seismic data QC and Conditioning

Step	Checked/ not checked	Qc Results
Zero phase QC	Checked	All three seismic cube are zero phase
Time Shift QC	checked	Far section is time shifted to about -6ms (correction was applied)
Frequency and phase balancing	checked	Well balanced

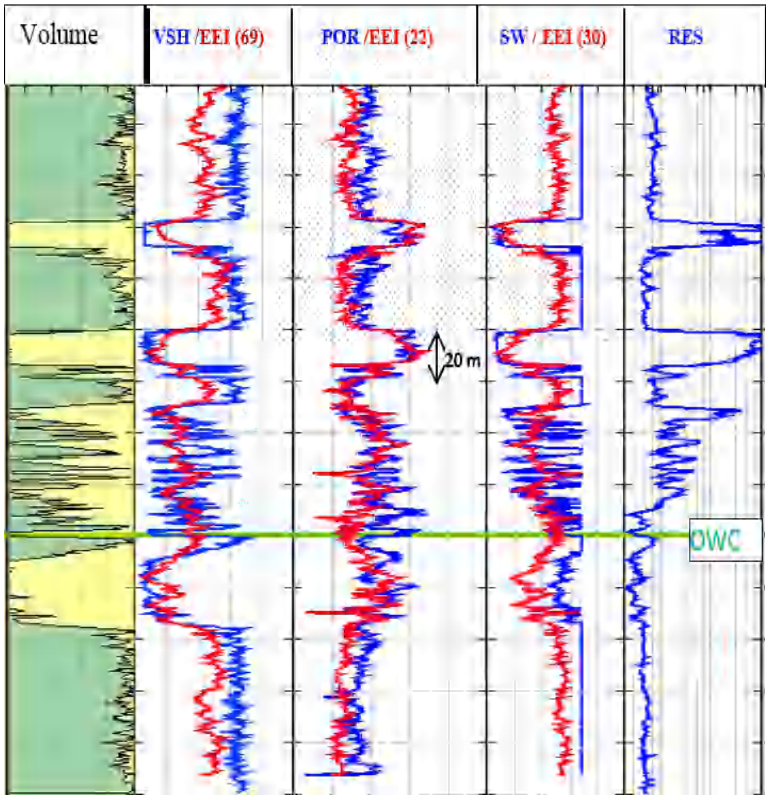

Figure 7: Comparison of petrophycal logs with logs derived from EEI using the optimum angle after normalization (Pu – 2B)

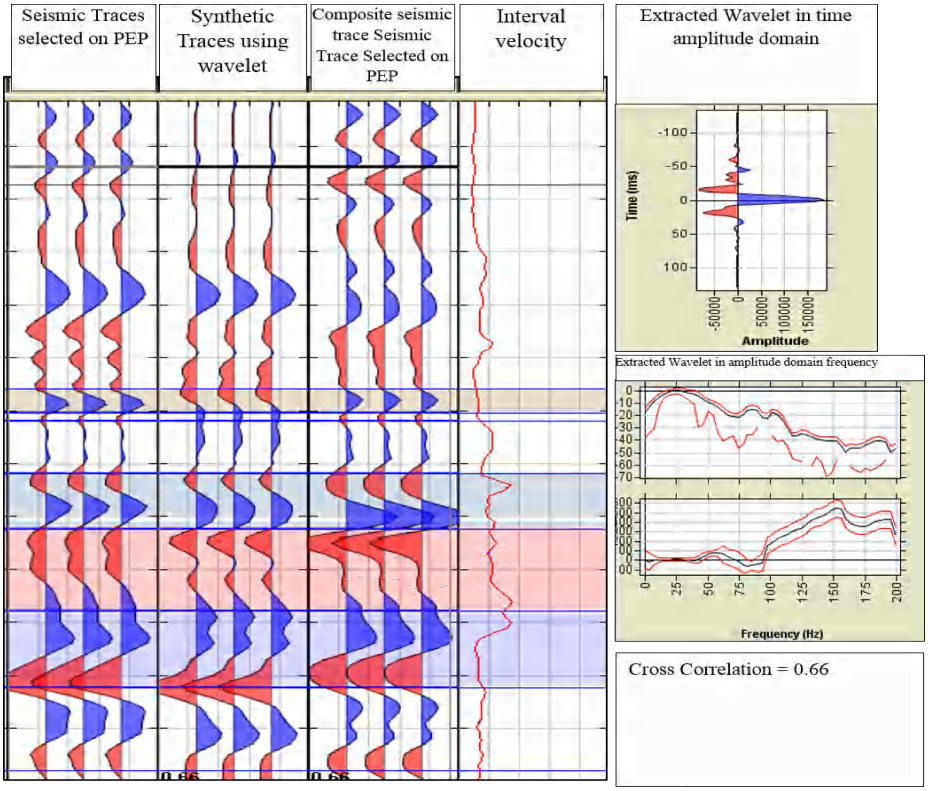

Figure 8a: Zero phased extraction of wavelet derived from near seismic and well ties (Pu – 2B)

Low Frequency Modeling

The low frequency model for this work was generated based on the works of Pauget, 2009, by application of automatic horizons. Thus, control horizons were used to refine automatic horizons for stratigraphic modeling as shown in (Figure 9a) and (Figure 9b). Hence in Figure 9c, P-wave velocity, acoustic and gradient impedence logs were interpolated based on stratigraphic controls. Hence, interpolated model was filtered in the rage 0-10 HZ low frequency range.This work applied the inverse distance based algorithm for inter polation based on 6 wells to build three background models (AI, GI and Vp) after which inversion began.

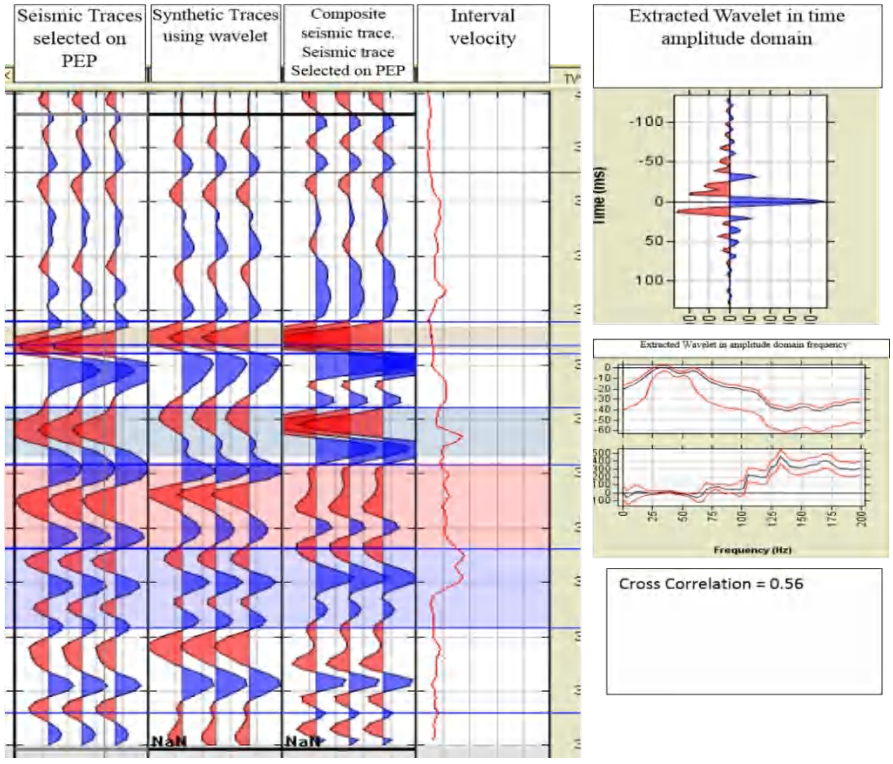

Figure 8b: Zero phased extraction of wavelet derived from far seismic and well tie (Pu – 2B)

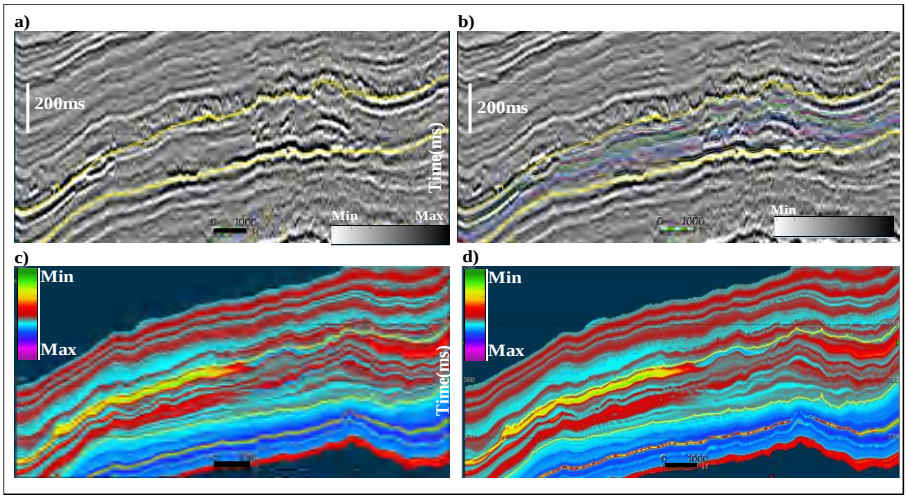

Figure 9: Stage wise process for generation of low frequency models: (a) control horizons applied to refine automatic horizons, (b)Auto-tracked horizons based on sequence stratigraphy,(c) elastic property interpolation along the auto-tracked horizons,(d) Generation of low frequency models and subsequent filtering.

Wavelet extraction and synthetic seismogram based on statistical/quantitative approach

Recall that the Near, mid and far partial stacks were applied prior to inversion in order to carry out seismic well tie. Hence a synthetic data was developed based on comparison between the real and seismic data in the time window, through a time depth relationship at every well for wavelet extraction. This extracted wavelet forms the basis of synthetic data (Nascimento, 2013; Salleh, 1999).

Seismic inversion result and QC

The Deterministic inversion model applied for herein is called the simultaneous model based inversion approach. Deterministic inversion is deemed fit for this work due the thickness volume of the area of study and the high reflectivity.

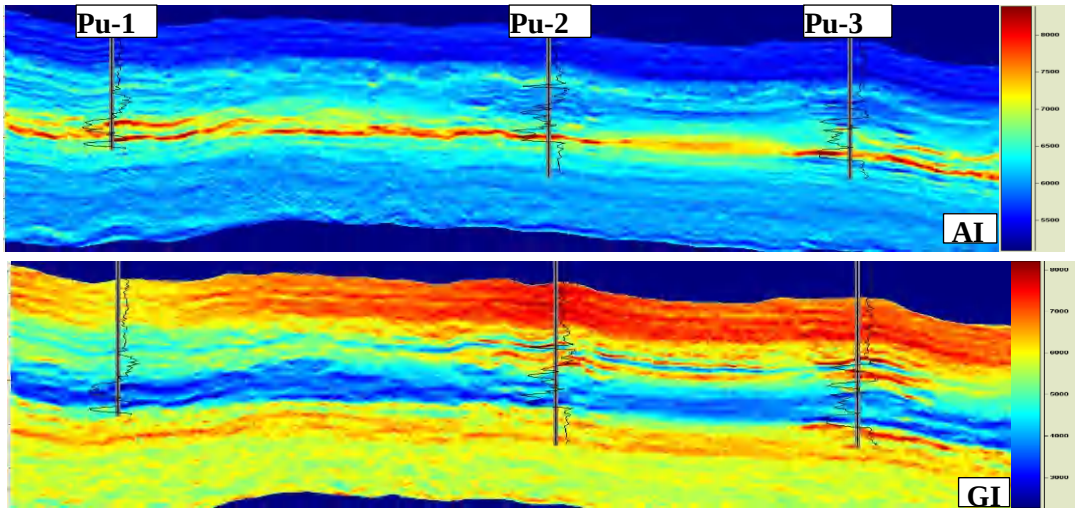

Figure 10: Sections passing though wells showing the inverted AI (top) and GI (bottom). The black curves overlain on the section are GR logs

To achieve result, an initial impedance model was continuously iterated and modified in order to fit properly with seismic race.

The initial model utilized herein include the interpolated impedance data from wells and guided by a stratigraphic framework defined by the pick seismic horizons. After convolving the AVO approximation equation of Wiggins et al. (1985) against wavelet W (θ), the synthetic seismic trace applied herein is written as;

$$S_{PP}(\theta) = a/2\,W(\theta)\Delta Ln(AI) + b/2\,W(\theta)\Delta\delta Ln(GI) + c/2\,W(\theta)\Delta\delta Ln(vp) \quad (11)$$

Where

$a = 1 + \alpha_{GI}b + \alpha_{Vp}c, \quad b = sin^2\theta, \quad c = sin^2\theta tan^2\theta$

α_{GI} gradient coefficient of GI (in y axis) versus AI(in x axis)

α_{Vp} gradient coefficient of V_p (in y axis) versus AI(in x axis)

$\delta Ln(V_P)$ deviation from the linear equation V_p (in y axis) versus AI(in x axis)

$\delta Ln(GI)$ deviation from the linear equation GI (in y axis) versus AI(in x axis)
$\delta Ln(GI)$ deviation from the linear equation GI (in y axis) versus AI(in x axis).
In the matrix form, Equation 11 is reduced to;

$$S = J \cdot Ln(Z) \qquad (12)$$

J is the system matrix of the product of W and D.
The diagonal matrix D is composed of the difference operation Δ, applied to each Ln (AI), $\delta Ln(V_P)$ and $\delta Ln(GI)$. Column vector Ln (Z) is composed of Ln (AI), $\delta Ln(V_P)$ and $\delta Ln(GI)$. W is a banded matrix composed of extracted wavelets per partial angle stack. S is a column vector of the near, mid and far seismic traces.
To solve Equation 12 for Ln(Z), the following total objective function is minimized;

$$\|S_{real} - X \cdot Ln(Z)\|^2 + \mu \ \|Ln(Z) - Ln(Z_0)\|^2 \qquad (13)$$

Where μ is the model weight, it has to be small to guarantee the inversion is driven by real seismic data.Z_0 is the initial model with which the inversion starts.

The conjugate gradient method is used to iteratively modify Ln(Z) until the difference between the synthetic seismic data $S_{pp}(\theta)$ and real seismic data $S_{real}(\theta)$ is minimized for near, mid and far stack angles. It is then straightforward to derive Z by exponentiation of Ln(Z)
The gradient and acoustic inversion result are depicted in Figure 10, this is showing a section cutting across three (3) wells and expressed by gamma ray logs. A deliberate ommition of Pu 1A was done in order to make it a blind test well while others were applied for generation of background low frequency model. Coefficient between inverted and initial loges were found to be 0.09 for AI and 0.82 for GI ans depicted in Figure 11. Correlation factors and inversion result presented acceptable data at the blind test well thus demonstrating high quality of inversion studies.

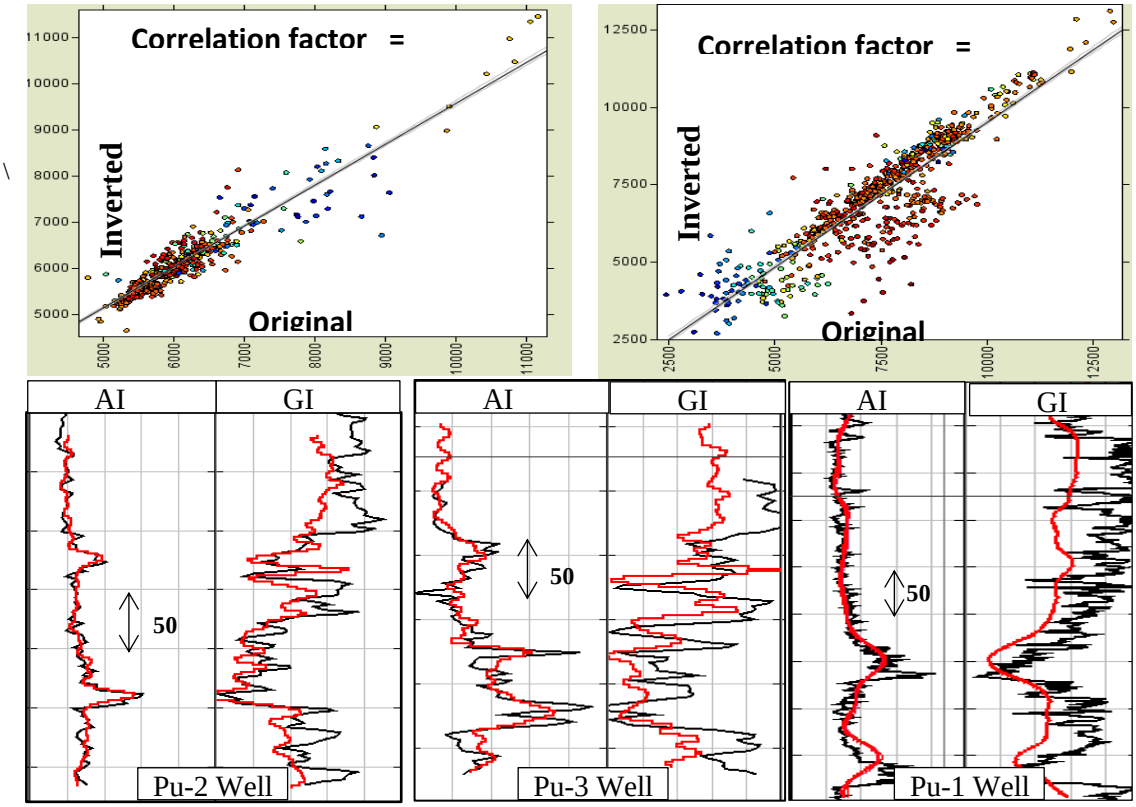

Figure 11: Quality Control applied on results: (Top) Inverted seismic impedances versus well log impedances; (bottom) Comparison of Inverted AI & GI (in red color) with initial well log measurements (in black co lor)

Computation of equivalent EEI volume through (Equation 10)
Now that initial well log measurements match with inverted seismic data, it is convenient to transform inverted impedences into EEI volumes based on equation 7 in consideration with the optimal angle derived from section 3.2.1. Target interval bounding horizons were applied for calculations of normalization factor AI_0. Optimal angles of $\chi = 22^o$,and 69°, were computed based on (Equation 7) get the EEI volumes as in Figure 6. As depicted in Figure 12, two sections passing through wells are EEI for $\chi = 22^o$ (top of Figure 12), corresponding to porosity volume, while EEI for $\chi = 69^o$ (bottom of Figure 12), corresponds to shale volume. Note that the corresponding properties that were firstly derived from EEI (22^o) and EEI (69^o) well logs were overlain on each section, which revealed a correlation in honor of original data.

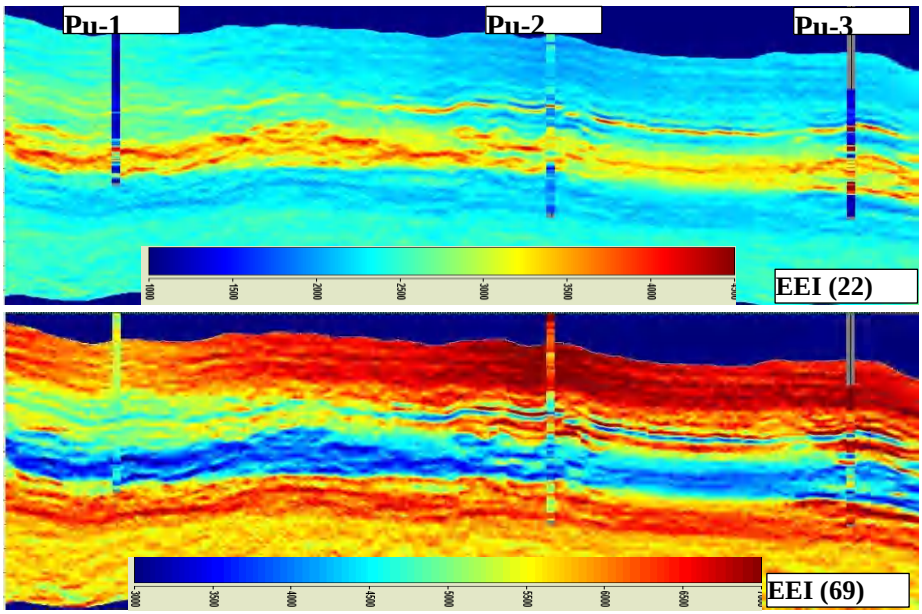

Figure 12: Sections passing though wells indicating EEI at $\chi = 22^{o}$ (top), corresponding to porosity volume. While EEI at $\chi = 69^{o}$ (bottom), corresponds to shale volume.

The corresponding EEI curve for water saturation (Sw_{eff}) was not applied due to its in ability to provide a good match with the well log.

The water saturation curve was not applied as a result of its incapacity to match the well log.

Hence, based on Figure 12, sand reservoirs can be well mapped by mapping areas of high impedance at EEI (22°) and the areas of low impedance at EEI at (69°).

This is clearly proving the ability of EEI approach in mapping reservoir sands from those EEI derived petrophysical properties.

Derivation of uantitative petrophysical properties from EEI volumes

A cross plotting of extended elastic impedance log dada was carried out in 3 dimensional space and a linear trend was presented by different lithologies. A clor coded approach for porosity and shale volume was conducted and applied to convert EEI volumes into shale content and porosity volumes as presented in Figure 13. Locations where contour lines are less than 3640ms and presented a high porosity and loweshale content are termed as favorable zones. An observation of (Figs. 13) reveals that the reservoir is clearly defined by high shale volume. Also, high values of porosity which should be related to the presence of reservoir were also observed.

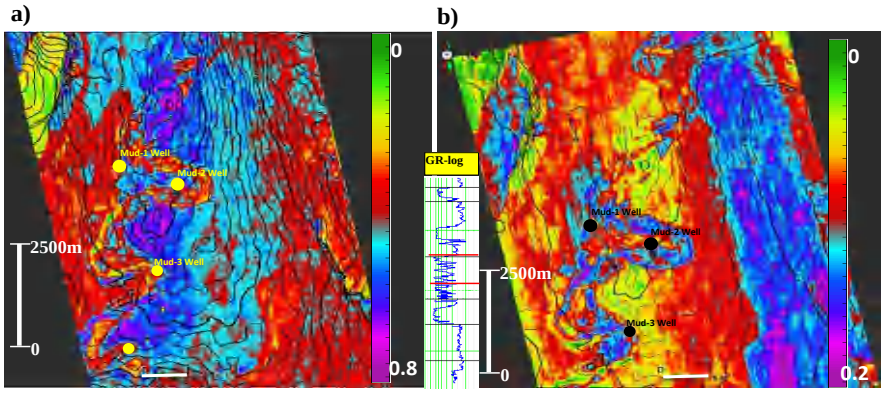

Figure 13: Top and bottom section of the o73 (captioned by red lines on GR-log) with the shale volume (left) and porosity content (right). Areas where contour lines are less than 3640 with high porosity and lower shale content are declared as favorable zones.

Facies distribution derived from Minimum Energy Angle

One of the major contribution of this work is the application of Minimum energy Angle to derive reservoir facies distribution by isolation of oil reservoir sand from non-reservoir facies. This concept was explained in previous literature review conducted by this paper and presented by equation 10.

In this research, a minimum energy was range was observed by creating an EEI log spectrum for a range of angles from χ = -90° to χ= +90° based quality well log analysis. Hence a rigourous analysis of the spectrum was conducted and a minimum energy was located at exactly 22° as depicted by (Figure 14). Hence, it suggests that at χ = 22°, the variation in the log property for top non reservoir facies is at minimum, and thus considered as minimum energy angle.

In order to point out oil sand reservoir facies, distribution for background EEI as presented in (Figure 16) and at well locations were properly analyzed and values for cut off criteria were then obtained, thus making a basis for volume calculation.

The lateral thick black line on (Figure 16) is the likely extension of oil water contact interpreted from wells. For this reservoir unit, the background EEI captured almost accurately the high EEI corresponding to water sand, while the oil sand reservoirs are characterized by low background EEI.

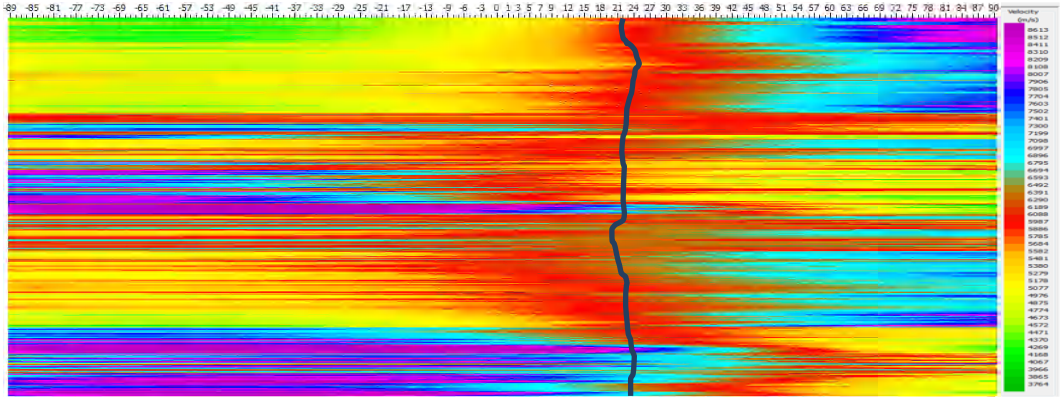

Figure 14: The EEI log spectrum at minimum energy x and at 22 deg. This corresponds to EEI log at the minimum energy angle which was applied together with the interpreted horizons to build a low frequency model and then subsequently to a model based deterministic inversion that was converted to absolute rock property

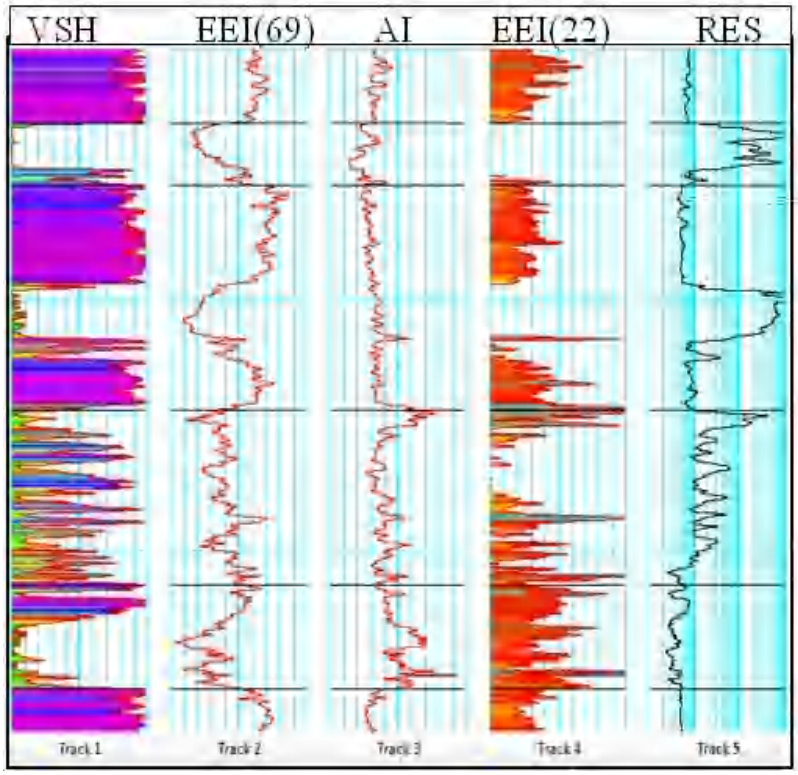

Figure 15: Comparison between EEI log at (x) and P-Impedance. It can be observed that the reservoir facies are more prominent at EEI (22) log

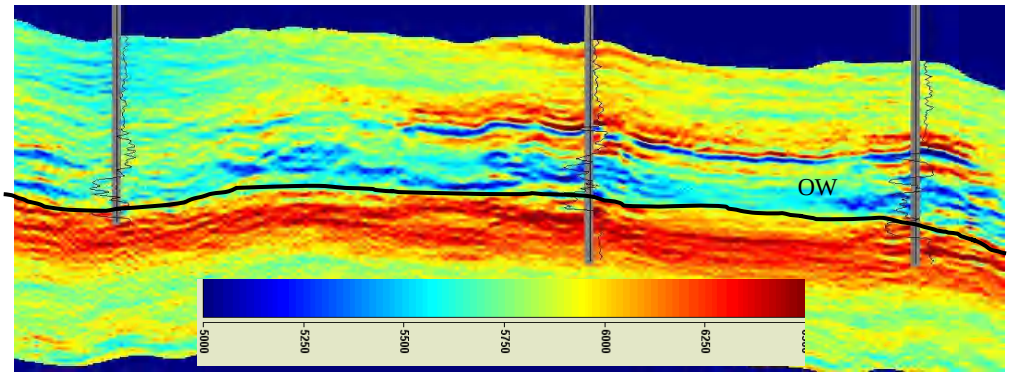

Figure 16. Well section indicating EEI at $\chi = 22^{o}$ and in correspondence to background EEI

Petrophysical Properties based on Conventional 3D Geo-statistical Modeling

To derive petrophysical properties based on conventional geostatisctis approach, different type of data were used; well logs, core reports, and production data. From these raw data models data were built (Core data, seismic data, conceptual geologic data, , well test and production data. Well log curves were provided for all wells. Raster image log curves were utilized from four wells. The geophysical log suite for this study varied among the utilized wells but generally included combinations of caliper log, neutron porosity log, gamma ray log and other curves, including resistivity and density. Although core analysis data were provided for three major cored wells (Pu-1A, Pu-2B and Pu-2A), in which all of the three wells had digital logs. The core analysis data include that of porosity, water saturation data, permeability data, grain density, and lithologic descriptions data.

The steps used to derive petrophysical properties consist of conducting a petrophysical analysis by integrating well log and core analyses, developing a structural model that integrates the stratigraphic framework and fault system of the reservoirs so as to capture the morphology of the study area. Then, building a distribution models of sedimentary microfacies (or sand bodies) on the basis of drilling and logging data, isochronous stratigraphic correlation unit (as the framework), dynamic integration of parameters and characteristics of channel sand bodies a well as analysis of variation function. This was followed by the application of the models of sedimentary microfacies (or sand bodies) to build models of reservoir property parameters and to determine a rational model on the basis of stochastic simulation. Finally, author's applied the statistical sequential Gausian simulation stochastic modelling to evaluate the static distribution of reservoir petro-physical properties on the bases of the developed facies models, thereby developing maps of Porosity and Net to Gross ratio (NtG).

Structural Modeling

The overall structural model developed herein is the integration of fault model and bedding simulation results generated in the revious sections. This is used for 3-D display of plutonion fields reservoir block's structure. During bedding simulation, the impact of fault was not considered. Therefore, relevant results generally showed local smooth near the fault. The impact of fault was taken into account in the overall structural modeling. As such, during the overall structural modelling, fault surface was used to filter previous bedding results.

During the filtering of faults, the bedding was changed into point data, considering the unreasonable degree of data on both sides of the fault surface, , a certain distance was allocated, thereby deleting unreasonable data, and then the filtered feasible point data type was achieved. After conducting such filtering on each bedding, the final point data type were then used to make an overall structural model. The final result of the overall structural model is illustrated in (Figure 17), thus recovering the structure-related data and maps for future application in facies and property models as well as the dynamic reservoir simulation.

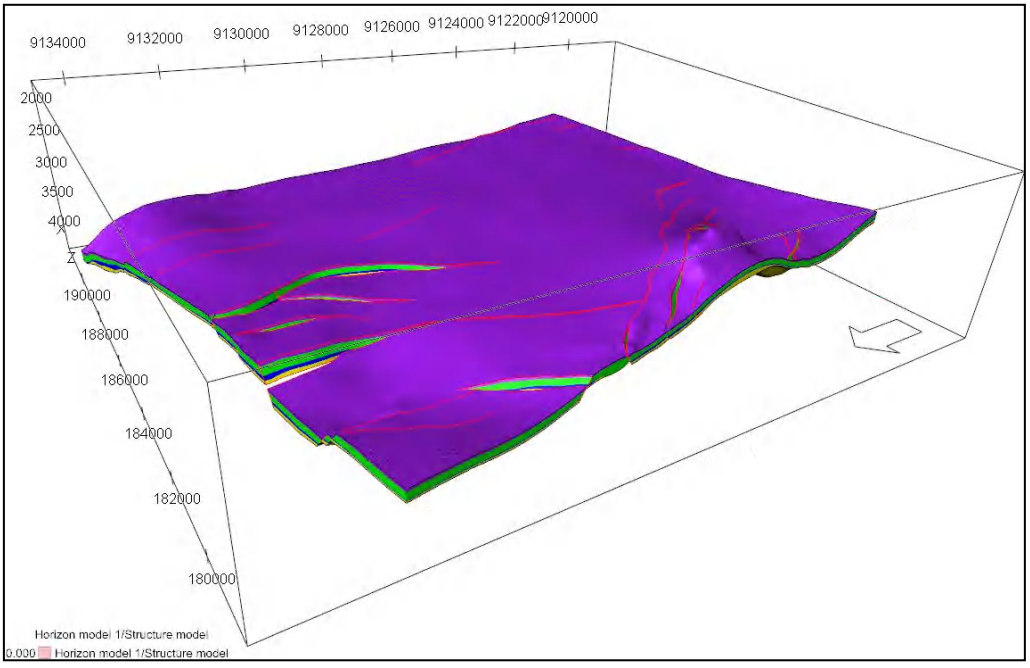

Figure 17: Overall Structural Model

Facies Modeling

Identification of sedimentary microfacies

As a starting point, this work began with the identification of the sedimentary microfacies with respect to single well.The division is mainly based on the cross plot between gradient impedance (GI) and velocity ratio of the longitudinal wave to that of the transverse wave (Vp/Vs). The colour of porosity was considered as the demarcation criteria as shown in (Figure 18), in which red dot represent a low porosity value, and bluish violet represents a high porosity value. Many authors (Adams, 2005; Anna et al., 2009) have described the intricate and various methodologies applied in such type of sedimentary microfacies analysis.

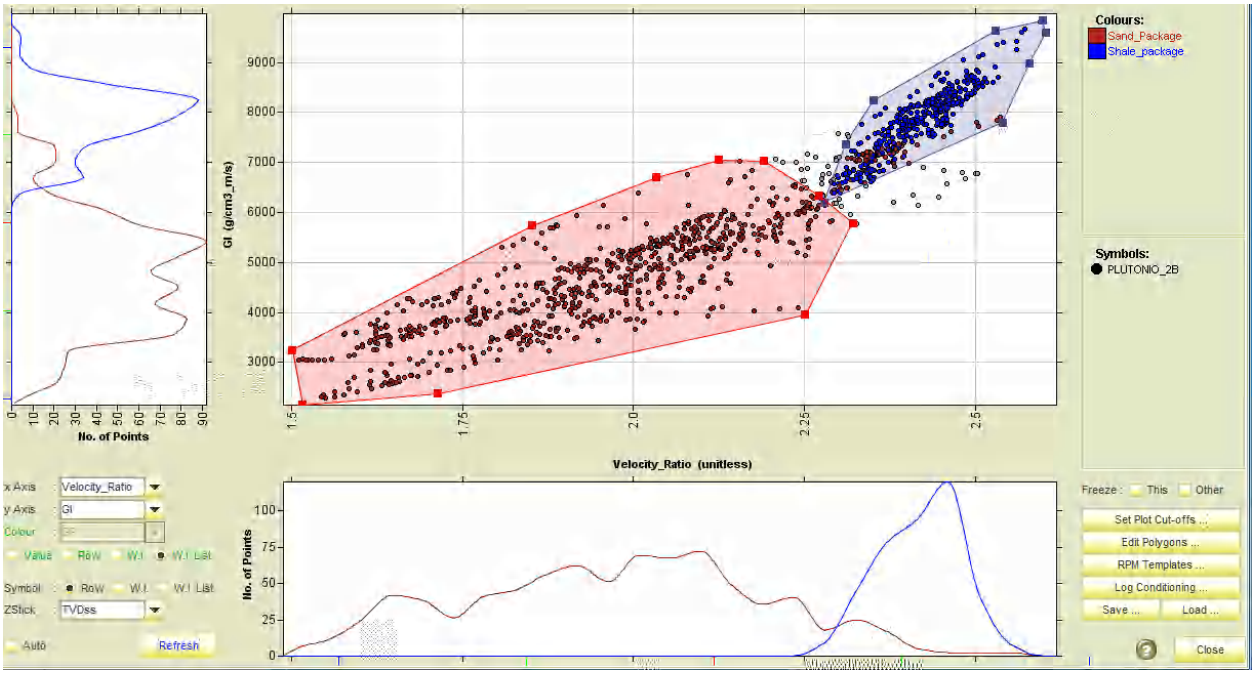

Figure 18: Cross plot of wave impedance curve (AI) and curve of velocity ratio of the longitudinal wave to that of the transverse wave (VPVS)

Microfacies (lithology) identification derived by this cross plot was used to automatically generate a microfacies (lithology) curve, which mainly distinguishes three microfacies, i.e. mudstone (Shale), turbidite channels and sheet sand facies. The standard sand-mudstone curve was used as a QC, in order to ensure the consistency with microfacies curve derived. This is shown in (Figure 19). It depicts microfacies boundary primarily on the basis of the division result of single well and distribution diagram with respect to thickness of sand bodies.

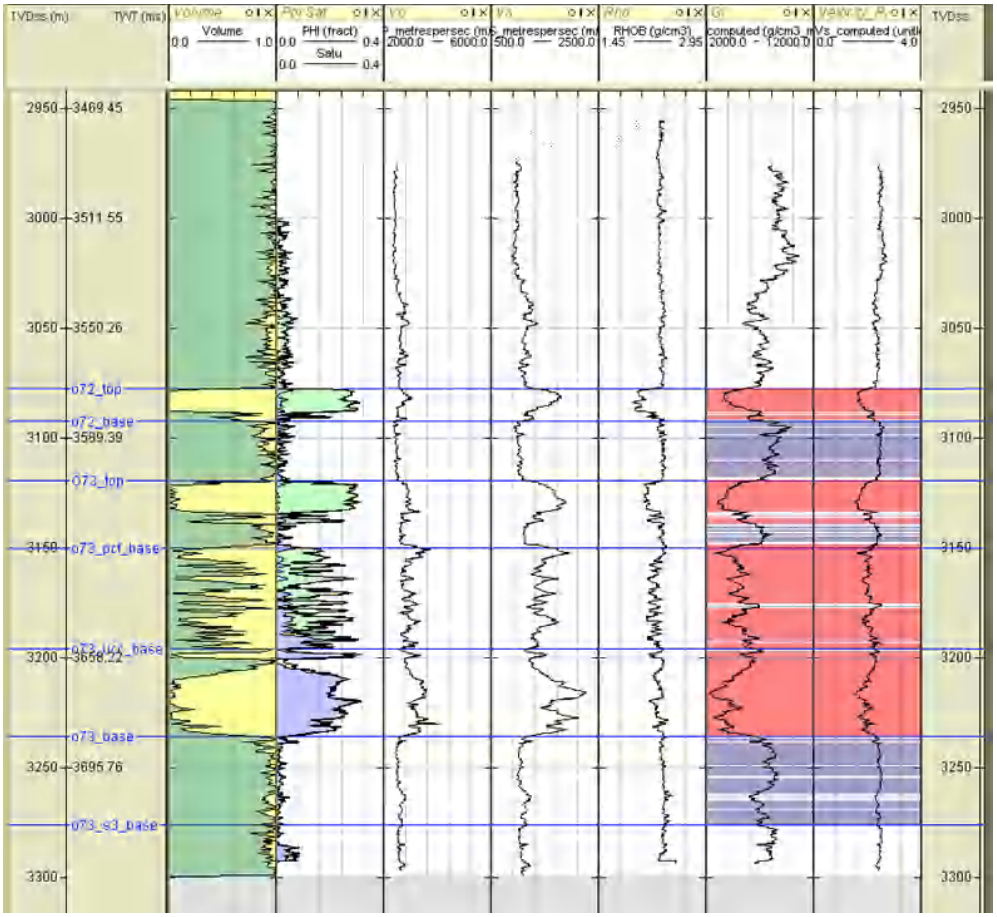

Figure 19: Sedimentary microfacies curve on single well

Geological trend body

The sequential indicator simulation in establishing the tendency of sedimentary microfacies identified in the previous section was applied. The idea of converting geological knowledge into trend is the primary objective. It therefore translated the distribution regularities of plane and vertical facies into trend parameters, so as to establish a bases for microfacies (sandbody) modelling.

Plane distribution trend of sedimentary microfacies (sand body)

Plane trend of a sedimentary microfacies is the regularity of changes in plane with regards to the ratio of thickness of sedimentary microfacies to the thickness of single layer where such microfacie resides. In other words, it is the plane distribution of thickness percentage of sedimentary microfacies (Mardani et al., 2013; Masoudi et al., 2011; Pettingill, 1998). The plane distribution of facies thickness percentage was determined, as shown in (Figs. 20 to 21), on the basis of:

i. Plane figure thickness of sand body of each single layer from the results of previous geological researches
ii. Distribution area of each microfacies; and
iii. Changes in thickness of each microfacies.

Having cited the plane trend, the software application applied herein automatically converts the plane trend into 3D trend body.

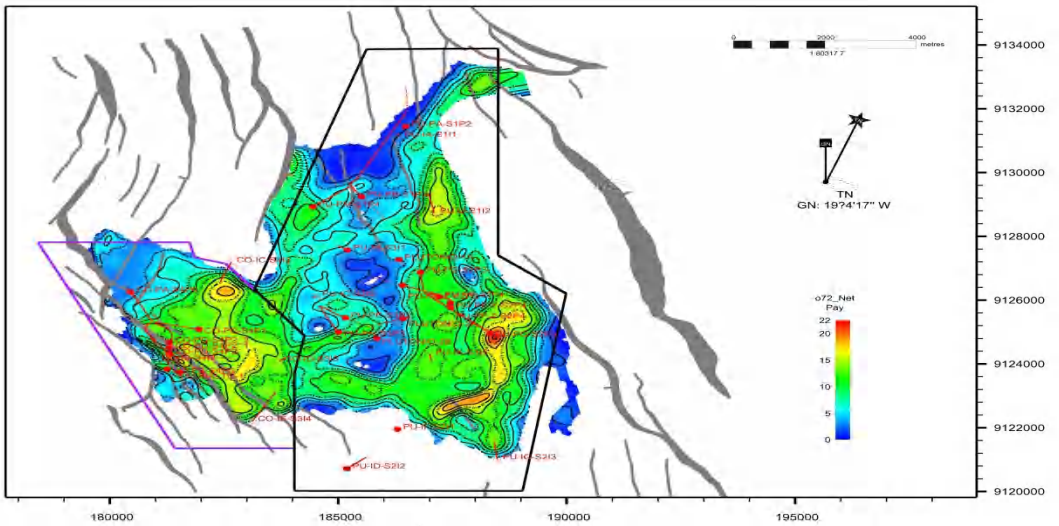

Figure 20: Plane figure of percentage thickness of o72 sand body composing mainly of sheet sand

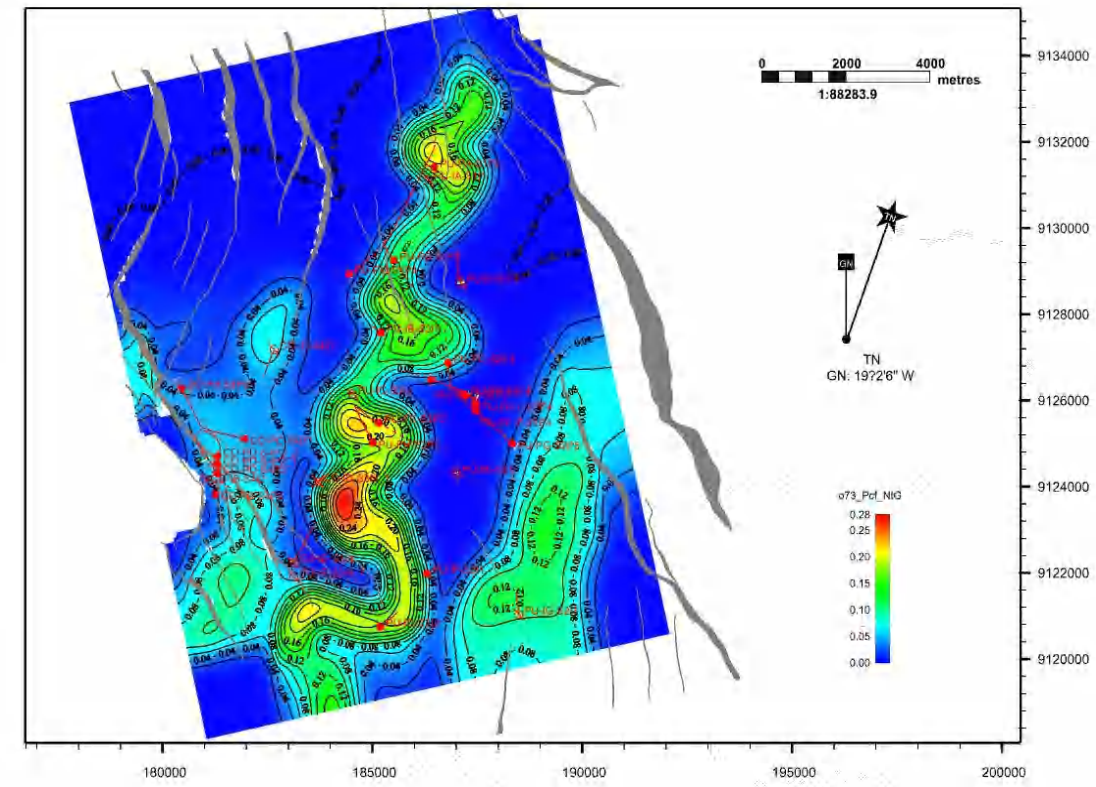

Figure 21: Plane figure of percentage thickness of o73_pcf sand body showing the presence of turbidity channel and sheet sand facies

Vertical trend body of sedimentary microfacies

The vertical trend is a 1D trend that shows the percentage of different microfacies (or lithology) on every layer placed vertically on the grid body. This trend body is based on well data analysis result. Therefore, If there are few wells, the accuracy of 1D trend body will be relatively low. But decision is made on whether or not to apply it based on the prevailing geological condition.

Facies trend distribution

Based on the above vertical trend, one can understand that the 3D trend body (i.e. plane trend) can be used for controlling the distribution and thickness changes of different microfacies in every geological layer while the vertical or 1D trend body is mainly used for controlling the percentage of different microfacies in each subdivided layer. In general, 3D trend body and 1D trend body are both used for restraining the simulation of sedimentary microfacies, but when there are few wells, the accuracy of 1D trend body after geo-statistics is characterized by a relatively low value (Huang et al., 2011). In this research, there are no such many wells, thereby resulting to a wide spacing and the accuracy of 1D trend body after geo-statistics was found to be relatively low. Therefore, we applied only the result of 3D (Plane) trend body as a bases for microfacies simulation.

Stochastic simulation was applied rather than pure calculation for description of channels and thickness changes. By doing so, the work is not only ensuring the consistency with the previous geological knowledge, but also use the advantage of stochastic simulation to depict the distribution of sand bodies. In general, the microfacies simulation is based on the geological knowledge and is conducive for model updating in the future.

Property model

One of the most important aspects of reservoir modeling is the simulation of reservoir properties. Main reservoir physical properties affecting the exploitation of oil and gas are porosity, permeability and water saturation. With regards to this research, Property model was developed under the control of sedimentary microfacies. Hence, sequential Gaussian stochastic simulation was used to simulate the spatial distribution of porosity and permeability in the field.

Cut-off Determinations

The shale volume and porosity cutoffs were applied herein to evaluate net sandstone thickness in well logs. Net-sand thickness is defined as that part of the gross rock thickness that contributes to hydrocarbon production. From the available production tests data, core analyses data and well logging interpretation conducted, the cut-offs of revoir net pay thickness can been determined based on (Table 2). Incorrect cutoffs will provide anomalously high or low calculated reservoir volume.

However, there is no universally accepted approach of determining cutoff with accuracy. Hence, in this study, effects of a number of possible cutoffs for approximately 20 wells that have reliable digital GR curves were analyzed, and net sand thickness was define as the sand interval with porosity > 13% (equals Vsh of 48%)

Table 2: The cut-offs of net pay thickness

Types	**Porosity (%)**	**S_O (%)**	**SH (%)**	**DEN (g/cm^3)**	**CNL (%)**	**RT (Ωm)**
Gas sand	≥13	≥50	＜20	≤2.38	＜ 18	≥10
Oil sand	≥13	≥50	＜20	≤2.38	≥ 18	≥ 1
Oil-water sand	≥13	40～50	＜20	≤2.38	≥18	0.8-1.3
Water sand	≥13	≤40	＜20	≤2.38	≥18	＜ 1
Dry sand	＜13		≥20	＞2.38	≥18	

Porosity model

In this research however, consideration was made on the lithology distribution, but used a fixed value for calculation. In other words, the sandstone grid of each single layer was assigned with an average value of porosity of such single layer. Porosity model herein is simulated upon;

i. Cut off value and full consideration to the impact of lithology distribution on porosity
ii. The stochastic simulation
iii. Relevance scope of variation function.

Validating the Extended Elastic Impedance Approach

Porosity

On comparison of the porosities derived from Geo-statistics with the porosity derived from the EEI volume from the o73-pcf reservoir section, as depicted on Fig 22., a clear conformity is observed between the two, which revealed a turbidity channel like distribution and some sheet sand.

Shale volume

Comparison between EEI derived shale volume and Geostatisctics model revealed a similarity as depicted in Fig; 23. When this is further compared with sand thickness derived in Figure 13, a clearer conformity is observed with the facies derived based on EEI at Minimum angle.

This comparison further validate the Extended Elastic Impedance Theory developed by (Whitecombbe et al 2002) in which a dominant sheet sand distribution can be observed from both figures. Unlike the dominant turbidity channel like of o73. This revealed that the EEI approach or methodology adopted by this research is capable of fully representing the field's reservoirs heterogeneity, thereby becoming acceptable as well as reliable in characterizing petroleum reservoirs.

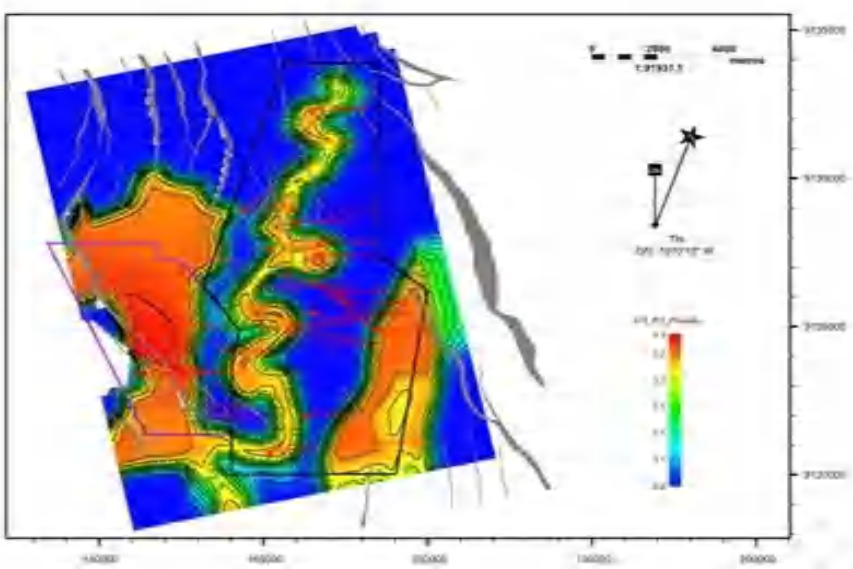

Figure 22: Plane figure of percentage Porosity of o73 sand body showing the presence of turbidity channel reservoir and sheet sand facies

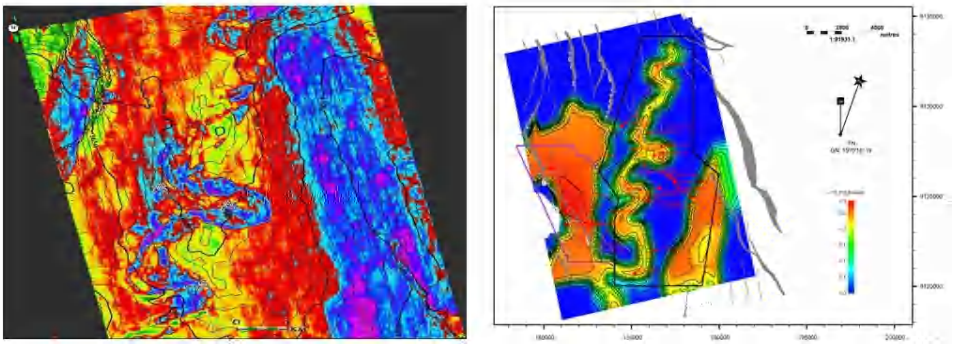

Figure 23: Comparison of percentage Porosity of o73 derived from EEI (left) and Geo-statistics (right). Showing the presence of turbidity channel reservoir and sheet sand facies

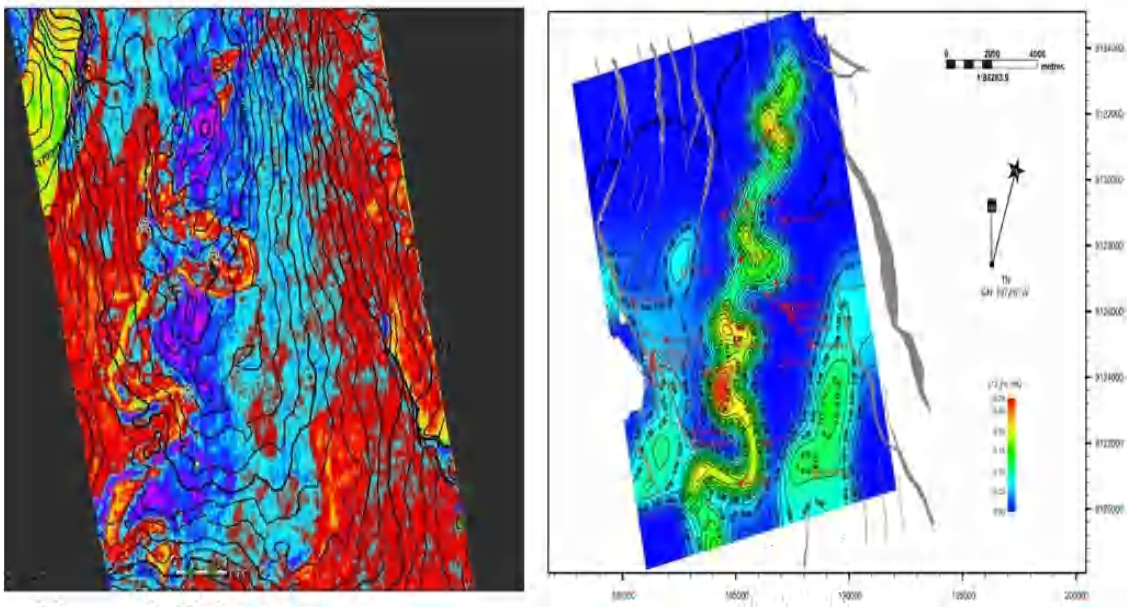

Figure 24: Comparison of percentage Volume of Shale of o73, derived from EEI (left) and Geo-statistics (right). Showing the presence of turbidity channel reservoir and sheet sand facies.

CONCLUSION

This case study revealed that Petroleum Reservoir sand can be mapped away from wells control using petrophysical property volumes derived from extended elastic impedances especially when computed at minimum energy angles. It has also revealed that porosity, EEI background and shale content

volumes can be used to pinpoint favorable hydrocarbon zones. Thereby delineating and identifying reservoir boundaries more accurately than using only acoustic impedance. A validation of the EEI method was conducted based on comparison between EEI based models and models derived from conventional Geo-statistical approach, which has further proved the reliability of the EEI methodology.

REFERENCES

Connolly P. (1999). Elastic Impedance: The Leading Edge,[J] v. 18, p. 438-452.

Contreras O, Hareland G and Aguilera R. (2013). Pore Pressure Modelling and Stress Faulting-Regime Determination of the Montney Shale in the Western Canada Sedimentary Basin: Journal of Canadian Petroleum Technology[J]. v. 52, p. 349-359, 2013.

Doyen, P.M. (2009). Porosity from Seismic data: A geostatistical approach. Geophysics, 53: 3963-3975.

Dubucq, D.B., S. Van Riel (2001). Turbidite reservoir characterization: Multi-offset stack inversion for reservoir delineation and porosity estimation; a Gulf of Guinea example, 71st Annual International Meeting, Soceity of Exploration geophysics, pp. 609-639.

Francis A M. (2002). Deterministic inversion: Overdue for retirement, PETEX: London, PETEX.

Francis A M. (2006). Understanding stochastic inversion: First Break, v. 24, p. 69-77.

Hicks. (2006). Extended Elastic Impedance and its relation to AVO crossploting and Vp/Vs: EAGE (Extended Abstract).

Iske T And T Randen.(2006). Atlas of 3D Seismic Attributes, Mathematics in Industry, Mathematical Methods and Modelling in Hydrocarbon Exploration and Production:[J]. Berlin, Springer.

Kemper M. (2010). Rock Physics driven inversionThe importance of workflow: First Break,[J] v. 28, p. 69-81.

Latimer R. (2000). An interpreters guide tounderstanding and working with seismic derived acoustic impedance data: The Leading Edge, v. 19, p. 242-256.

Mohsen Alebouyeh, Ali Chehrazi. (2018). Application of extended elastic impedance (EEI) inversion to reservoir from non-reservoir discrimination of Ghar reservoir in one Iranian oil field within Persian Gulf, Journal of Geophysics and Engineering, Volume 15, Issue 4, August 2018, Pages 1204–1213, https://doi.org/10.1088/1742-2140/aaac50.

Pauget, F., S.Lacaze, And T. Valding. (2009). A global approach to seismic interpretation base on cost function and minimization, 79th Annual International Meeting, SEG, Expanded Abstracts, pp. 2592–2596.

Samba, C., Lu, H. & Mukhtar, H (2017). Reservoir properties prediction using extended elastic impedance: the case of Nianga field of West African Congo basin. J Petrol Explor Prod Technol 7, 673–686 (2017). https://doi.org/10.1007/s13202-017-0328-0

Whitecombe D and Connolly P. (2002). Extended Elastic Impedance for Fluid and Lithology Prediction: Geophysics, [J]v. 67, p. 63-67.